Computational study on the structural features, vibrational aspects, chemical shifts, and electronic properties of 1,4-Dinitrosopiperazine-2-carboxylic acid: Insights into donor-acceptor interactions and thermodynamic properties

S. Selvaraj [a, *]

[a] Department of Physics, Saveetha School of Engineering, Saveetha Institute of Medical and Technical Sciences (SIMATS), Thandalam, Chennai, 602105, Tamil Nadu, India.
*Corresponding Author Email: sselvaphy@gmail.com

Abstract: This study employs computational simulations to comprehensively investigate the molecular properties of 1,4-Dinitrosopiperazine-2-carboxylic acid. Through rigorous analysis, the research explores the compound's structural characteristics, vibrational assignments, chemical shifts, electronic properties, donor-acceptor interactions, Mulliken atomic charges, molecular electrostatic potential surface (MESP), and thermodynamic parameters. The findings provide intricate insights into the behavior of the compound, unveiling potential applications in diverse chemical contexts. This thorough examination contributes significantly to our understanding of the fundamental properties of 1,4-Dinitrosopiperazine-2-carboxylic acid, offering invaluable knowledge for both further research endeavors and practical applications. The detailed elucidation of these properties holds promise for advancements in various fields, from pharmaceuticals to materials science, marking a significant stride towards harnessing the full potential of this compound in contemporary chemistry.

Keywords: Carboxylic acid, Piperazine, DFT, NBO, HOMO-LUMO, MESP

1. Introduction

Carboxylic acids are a diverse group of organic compounds with essential roles in various biochemical, industrial, and everyday processes. They are characterized by the presence of a carboxyl group (-COOH), which consists of a hydroxyl group (-OH) and a carbonyl group (C=O) bonded to the same carbon atom. These compounds can be easily derived from raw biomass sources like used frying oils and animal lipids [1-2]. Additionally, carboxylic acids exhibit a broad range of chemical reactivity, enabling them to participate in processes like esterification, amidation, and decarboxylation, making them highly practical in organic synthesis. Carboxylic acids find indispensable applications in chemistry, biochemistry, and various industries due to their remarkable versatility [3-6]. Piperazine, an organic heterocyclic compound, is distinguished by its six-membered ring featuring two nitrogen atoms situated at opposite positions. Blends containing piperazine, known for their enhanced solvent performance, have the potential to form stable and carcinogenic compounds via nitrosation, underscoring the importance of using them with care [7-12].

1,4-Dinitrosopiperazine-2-carboxylic acid, with the chemical formula $C_5H_8N_4O_4$, is a derivative of both piperazine and carboxylic acid. This heterocyclic compound holds significant importance in contemporary chemistry due to its intriguing properties, which have promising applications across various fields such as materials science and pharmaceuticals [13-15]. The molecule features a piperazine ring, a six-membered heterocyclic ring containing two nitrogen atoms, situated at its core. This ring's arrangement of two nitrogen atoms resembles a hexagon due to their opposing placement. The piperazine ring possesses two nitro groups (-NO2), characterized by their -NO2 configuration. Additionally, there is an extra carboxylic acid group (-COOH) attached to the piperazine ring, composed of a hydroxyl group (OH) linked to a central carbon atom and a carbonyl group (C=O).

Notably, there is a lack of prior computational research on this compound in the existing literature. It is crucial to gain an understanding of the fundamental properties of this substance to fully harness its potential. This research paper employs advanced computational simulations to conduct a comprehensive analysis of 1,4-Dinitrosopiperazine-2-carboxylic acid. The investigation encompasses various critical aspects, including

thermodynamic parameters, electronic properties, donor-acceptor interactions, Mulliken atomic charges, and structural characteristics. These extensive analyses provide crucial insights into the compound's behavior and potential applications.

2. Computational Methods

In the Gaussian 09W program package [16], the quantum chemical computations have been carried out using Density Functional Theory / Becke's Three parameters hybrid functional and Lee-Yang-Parr correlation (DFT/B3LYP) method with 6-311++G(d,p) basis set [17-19] to simulate the optimized geometrical parameters, vibrational frequencies, natural bond orbital (NBO), and Mulliken charge distribution of 1,4-Dinitrosopiperazine-2-carboxylic acid. Additionally, the Gauge-Invariant Atomic Orbital (GIAO) approach was used to compute the ^1H and ^{13}C NMR isotropic chemical shifts [20, 21] and the Time-Dependent (TD) DFT approach [22, 23] was used to predict the electronic properties of 1,4-Dinitrosopiperazine-2-carboxylic acid with same basis set. The visual presentation of the outputs, analysed using the Chemcraft program [24].

3. Results and Discussion

3.1. Insights into structural parameters

The optimized molecular structures of 1,4-Dinitrosopiperazine-2-carboxylic acid, with atom numbering, are graphically represented in Figure 1. Furthermore, precise details concerning bond lengths and angles can be found in Table 1. In the intricate electronic structure of 1,4-Dinitrosopiperazine-2-carboxylic acid, a rich tapestry of bond lengths and angles is unveiled. Seven distinct bond types, including oxygen - carbon (O-C), oxygen - hydrogen (O-H), oxygen - nitrogen (O-N), nitrogen - nitrogen (N-N), nitrogen - carbon (N-C), carbon - carbon (C-C), and carbon - hydrogen (C-H), were meticulously examined, each bearing its own unique characteristics. A singular O-H bond length was pinpointed at 0.970 Å, while the O-C, O-N, and N-N bonds revealed intriguing duality, ranging from 1.201 to 1.345 Å, 1.216 to 1.217 Å, and 1.341 to 1.342 Å, respectively. Further complexity arose with the C-C bond, which exhibited three distinct lengths within the span of 1.534 to 1.540 Å. Additionally, the N-C bonds exhibited four bond lengths, fluctuating between 1.455 and 1.465 Å, whereas the C-H bonds showcased seven distinctive lengths, spanning from 1.089 to 1.095 Å. Similarly, the electronic structure unravelled a captivating array of eleven bond angles, including carbon-oxygen-hydrogen (C-O-H), oxygen-carbon-oxygen (O-C-O), oxygen-carbon-carbon (O-C-C), oxygen-nitrogen-nitrogen (O-N-N), nitrogen-nitrogen-carbon (N-N-C), carbon-nitrogen-carbon (C-N-C), nitrogen-carbon-carbon (N-C-C), nitrogen-carbon-hydrogen (N-C-H), carbon-carbon-carbon (C-C-C), carbon-carbon-hydrogen (C-C-H), and hydrogen-carbon-hydrogen (H-C-H). Each bond angle offered a unique insight into the molecule's geometry. Notable measurements included a solitary C-O-H angle at 107.85°, an O-C-O angle at 124.41°, and a C-C-C angle at 110.97°. The O-C-C, O-N-N, and C-C-C angles exhibited intriguing dual ranges, spanning from 110.99 to 124.48°, 117.43 to 118.31-116.15°, respectively. Meanwhile, a trio of H-C-H angles revealed subtle variations, ranging from 108.98 to 109.19°, while four N-N-C bond angles presented diversity between 117.31 and 124.36°.
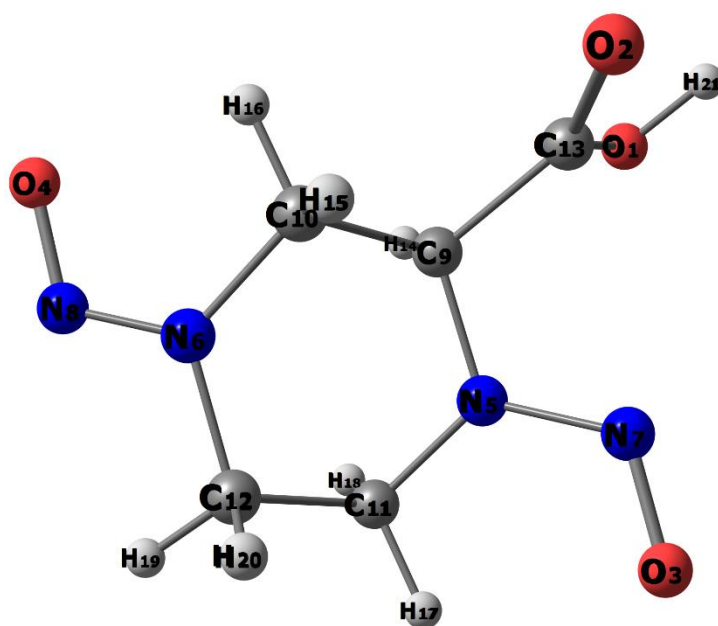

Figure 1. Optimized molecular geometrical structure of 1, 4-Dinitrosopiperazine-2-carboxylic acid

Table 1. Optimized geometrical parameters for 1,4-Dinitrosopiperazine-2-carboxylic acid

Bond lengths (Å)		Bond lengths (Å)	
O1-C13	1.345	C9-C10	1.540
O1-H21	0.970	C9-C13	1.534
O2-C13	1.201	C9-H14	1.095
O3-N7	1.216	C10-H15	1.093
O4-N8	1.217	C10-H16	1.089
N5-N7	1.341	C11-C12	1.535
N5-C9	1.465	C11-H17	1.089
N5-C11	1.464	C11-H18	1.095
N6-N8	1.342	C12-H19	1.090
N6-C10	1.460	C12-H20	1.095
N6-C12	1.455	-	-
Bond angles (∘)		**Bond angles (∘)**	
C13-O1-H21	107.85	N6-C10-C9	109.07
O1-C13-O2	124.41	N6-C10-H15	110.07
O1-C13-C9	110.99	N6-C10-H16	107.74
O2-C13-C9	124.48	N6-C12-C11	109.83
O3-N7-N5	116.15	N6-C12-H19	107.56
O4-N8-N6	116.15	N6-C12-H20	109.40
N7-N5-C9	117.82	C10-C9-C13	110.97
N7-N5-C11	124.36	C10-C9-H14	109.38
C9-N5-C11	117.43	C9-C10-H15	109.63
N5-C9-C10	109.67	C9-C10-H16	111.26
N5-C9-C13	110.95	C13-C9-H14	107.99
N5-C9-H14	107.80	H15-C10-H16	109.06
N5-C11-C12	109.35	C12-C11-H17	111.64
N5-C11-H17	107.29	C12-C11-H18	110.47
N5-C11-H18	108.81	C11-C12-H19	111.25
N8-N6-C10	124.14	C11-C12-H20	109.77
N8-N6-C12	117.31	H17-C11-H18	109.19
C10-N6-C12	118.31	H19-C12-H20	108.98

Furthermore, the five N-C-C bond angles displayed intriguing subtleties, oscillating from 109.35 to 110.95⁰, and the seven N-C-H and C-C-H bond angles showcased a broad spectrum of values within the range of 107.29 to 110.07⁰ and 107.99 to 111.64⁰, respectively. The computed values closely match previously reported standard values [25-31], affirming the accuracy of the calculations and providing robust validation for the theoretical predictions. This meticulous examination vividly illuminates the intricate structural nuances of this distinctive molecule. Moreover, by taking these factors into account, not only does it enhance our comprehension of the electronic configuration of 1,4-Dinitrosopiperazine-2-carboxylic acid, but it also underscores the broader implications of these structural intricacies within the domain of chemical science.

3.2. Vibrational properties

The precise vibrational assignments serve as both a cornerstone for future spectroscopic inquiries and a substantial contribution to comprehending the compound's chemical behavior and reactivity at a molecular scale. 1,4-Dinitrosopiperazine-2-carboxylic

acid comprises 21 atoms and exhibits 57 fundamental modes of vibrations, following the (3N-6) normal modes assumption under C_1 point group symmetry. The simulated IR and Raman spectra are illustrated in Figure 2, while the respective vibrational assignments are detailed in Table 2.

The vibrational spectroscopic examination of 1,4-Dinitrosopiperazine-2-carboxylic acid elucidates the nuanced interactions and energetic responses exhibited by its diverse functional groups. The prominent peak observed at 3753 cm^{-1}, attributed to the robust stretching vibration of the hydroxyl (OH) group, strongly implies its significant involvement in pivotal intermolecular interactions. Modes 2 through 8, denoting asymmetric stretching vibrations of methylene (CH_2) groups, underscore the dynamic behavior of these constituents within the molecular vibrational spectrum. This dynamic behavior suggests a potentially crucial role for CH_2 groups in governing the molecule's reactivity and potential affinity for binding with other molecular species. The vibrational band at 1825 cm^{-1}, attributed to the stretching motion of the carbonyl (C=O) group, not only affirms its presence but also implies its potential participation in electronic interactions. This is further supported by the high IR intensity, signifying the significance of this functional group within the molecule. Modes 10 and 11, resonating at 1564 and 1556 cm^{-1}, pertain to stretching vibrations associated with the nitro (NO) groups, coupled with concurrent vibrations linked to the methylene (CH_2) groups, suggest a complex interplay between these functionalities. The moderate to high IR intensities and Raman activities of these modes further emphasize their potential involvement in molecular interactions.

Modes 15 to 20, spanning the spectral range of 1419 to 1344 cm^{-1}, encompass vibrational modes associated with nitrogen-nitrogen (NN) bonds, hydroxyl (OH) bending, as well as a range of CH_2 bending modes. This intricate range of vibrations implies that these functionalities are not only present but are likely engaged in dynamic interactions within the molecular framework. Modes 21 to 55 introduce a wide array of vibrational modes involving different combinations of CH_2, OH, NO, CN, and CO groups. This complexity underlines the diverse nature of vibrational interactions within the molecule. The varying intensities and activities of these modes further highlight the nuanced vibrational behavior, providing insight into the potential reactivity and binding properties of the compound. These vibrational assignments are substantiated by extensive literature [32-39], reinforcing their validity and accuracy. Overall, this detailed vibrational analysis offers a comprehensive view of the molecular dynamics, shedding light on the potential roles and interactions of specific functional groups.
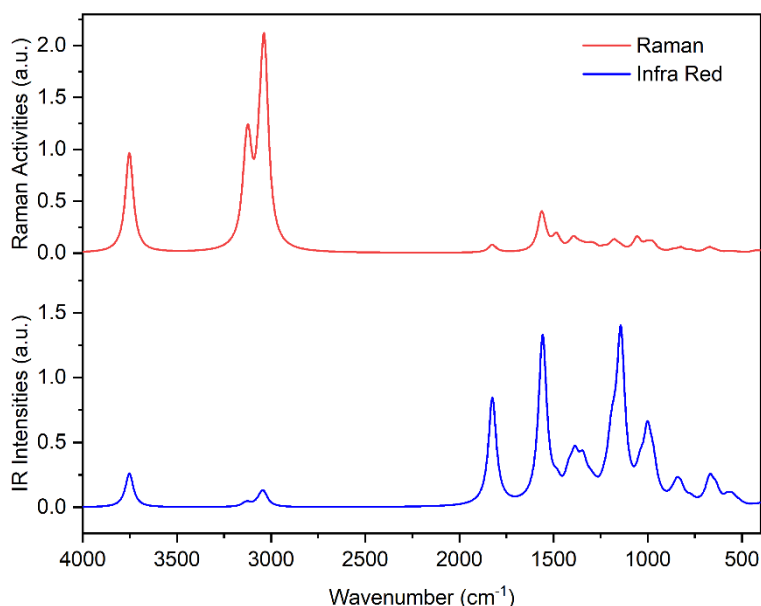
Figure 2. Vibrational spectra of 1,4-Dinitrosopiperazine-2-carboxylic acid

Table 2. Simulated wavenumbers and vibrational assignments of 1,4-Dinitrosopiperazine-2-carboxylic acid

Modes	Wavenumbers (cm^{-1})	IR intensity	Raman activity	Vibrational assignments
1	3753	97.70	151.29	υ OH
2	3136	6.52	33.87	υ$_{as}$ CH_2

3	3132	3.59	46.27	$υ_{as}$ CH_2
4	3120	3.78	97.04	$υ_{as}$ CH_2
5	3064	9.20	47.74	$υ_{as}$ CH_2, υ CH
6	3045	28.89	46.93	$υ_{as}$ CH_2, υ CH
7	3040	2.41	106.35	$υ_{as}$ CH_2, υ CH
8	3032	12.93	157.33	$υ_{as}$ CH_2, υ CH
9	1825	308.59	11.63	υ C=O
10	1564	116.86	46.45	υ NO, β NNO, □ CH_2, β CH
11	1556	372.14	14.80	υ NO, β NNO, □ CH_2, β CH
12	1489	2.81	11.79	□ CH_2
13	1482	25.22	2.72	□ CH_2
14	1480	8.61	8.47	□ CH_2
15	1419	58.29	2.21	υ NN, β OH, τ CH_2, β OH, ω CH_2
16	1395	6.32	14.89	τ CH_2
17	1387	89.28	2.13	ω CH_2
18	1375	4.42	1.15	ω CH_2, β CH
19	1360	15.34	4.84	ω CH_2, τ CH_2
20	1344	73.24	2.43	ω CH_2, τ CH_2
21	1330	14.73	2.99	υ CN, β OH, τ CH_2
22	1304	28.92	6.41	β OH, ω CH_2
23	1281	16.13	5.96	β OH, ω CH_2, β CH
24	1231	21.80	4.43	τ CH_2, β CH
25	1194	116.85	2.77	υ NN, τ CH_2, β OH
26	1177	55.80	13.05	υ NN, τ CH_2, β OH
27	1148	103.29	5.03	τ CH_2, β OH
28	1141	361.07	0.80	τ CH_2, β OH, β CH
29	1057	2.65	20.25	ρ CH_2
30	1039	64.67	1.12	ρ CH_2, β OH, β CH
31	1002	166.94	9.59	ρ CH_2, β OH, β CH
32	975	21.82	4.38	ω CH_2, β CH
33	970	66.48	6.84	ω CH_2, ρ CH_2
34	868	11.18	2.42	ω CH_2, ρ CH_2
35	845	44.25	1.22	ρ CH_2
36	823	31.31	5.85	ρ CH_2, υ CN
37	772	13.47	2.98	ρ CH_2, υ CO
38	688	2.17	1.65	ρ CH_2, β OH, β NO
39	671	68.51	6.15	ρ CH_2, β OH
40	639	40.27	2.34	β CH, β OH

41	575	19.27	1.14	ρ CH$_2$, β CH, β OH
42	548	20.18	1.38	β OH
43	515	7.74	0.60	ρ CH$_2$, β OH
44	431	2.64	2.20	ρ CH$_2$, β CH, β OH
45	397	2.34	0.90	ρ CH$_2$
46	375	6.84	1.43	ρ CH$_2$, β NO
47	351	4.95	1.52	ω CH$_2$, β OH
48	340	5.80	0.84	ω CH$_2$, β OH, β NO
49	320	0.63	6.34	ω CH$_2$, β OH
50	311	1.71	3.03	ρ CH$_2$
51	269	4.78	0.31	ρ CH$_2$, β NO
52	169	6.88	0.24	ρ CH$_2$, β CO
53	144	1.73	1.50	ρ CH$_2$, β CO, β OH
54	105	3.34	0.98	ρ CH$_2$, β NO
55	83	2.26	2.47	β NO, β OH
56	51	3.36	1.28	ω CH$_2$, β NO
57	15	5.21	0.47	ω CH$_2$, β NO
υ - stretching, υ_s - symmetric stretching, υ_{as} - asymmetric stretching, τ - twisting, ω - wagging, $\square$ - scissoring, β - deformation / bending				

3.3. Chemical shifts

The simulated ^{1}H (proton) and ^{13}C (carbon) spectra of 1,4-Dinitrosopiperazine-2-carboxylic acid were depicted in Figure 3. Meanwhile the Table 3 provides simulated chemical shift values (in ppm) with atom numbering corresponding to the arrangements in Figure 1, for specific atoms within 1,4-Dinitrosopiperazine-2-carboxylic acid, as determined through both DFT calculations and ChemDraw software. In the 1,4-Dinitrosopiperazine-2-carboxylic acid, the hydroxyl (-OH) and the methylidyne (CH) protons were predicted at 6.175 ppm and 4.133 ppm, respectively. The hydroxyl proton exhibits the highest chemical shift indicating a distinctive electronic environment or high electron density. The methylene (CH$_2$) protons and carbons were predicted in the range of 5.527 – 2.391 ppm and 50.900 – 39.059 ppm, which shows good correlation with literature values [40, 41]. In similar way, the carbonyl carbon (C13) showed a distinct peak at 171.40 ppm, and methylidyne carbon (C9) at 62.748 ppm. These chemical shift observations further supported by previous report [42, 43].

However, a notable observation is the disparity in hydrogen (H) shifts between the two methods. For instance, H21, H17, and H16 exhibit higher shifts in the DFT calculations compared to the ChemDraw values, possibly stemming from methodological discrepancies. Similarly, variations in shifts are also observed for H19,

H14, H20, H15, and H18, underscoring the sensitivity of chemical shifts to computational approaches. Regarding carbon (C) shifts, discrepancies between DFT and ChemDraw are evident, with C13 and C9 displaying notable differences. Specifically, C13 experiences a substantial shift in the DFT prediction, likely attributed to variations in electronic structure models. C12, C10, and C11 also demonstrate shifts that vary, emphasizing the impact of computational methodology on chemical shift predictions These results emphasize the pivotal role of the chosen computational approach in NMR data interpretation, underscoring the need for methodological uniformity to ensure precise predictions.

The reported chemical shift values offer crucial insights into the electronic structure and chemical environment of atoms in 1,4-Dinitrosopiperazine-2-carboxylic acid. This aids in detailed structural analysis and deepens the understanding of its reactivity and interactions with other compounds.

3.4. Electronic properties

The simulated excitation energies, wavelengths, and oscillator strength of 1,4-Dinitrosopiperazine-2-carboxylic acid are presented in Table 4, and the corresponding electronic spectrum in gas phase depicted in Figure 4.
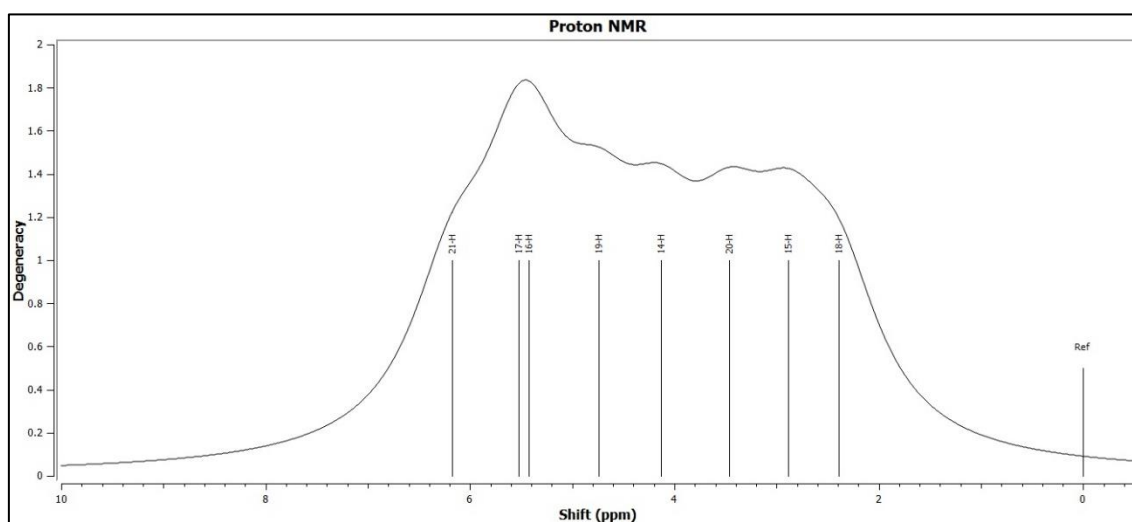
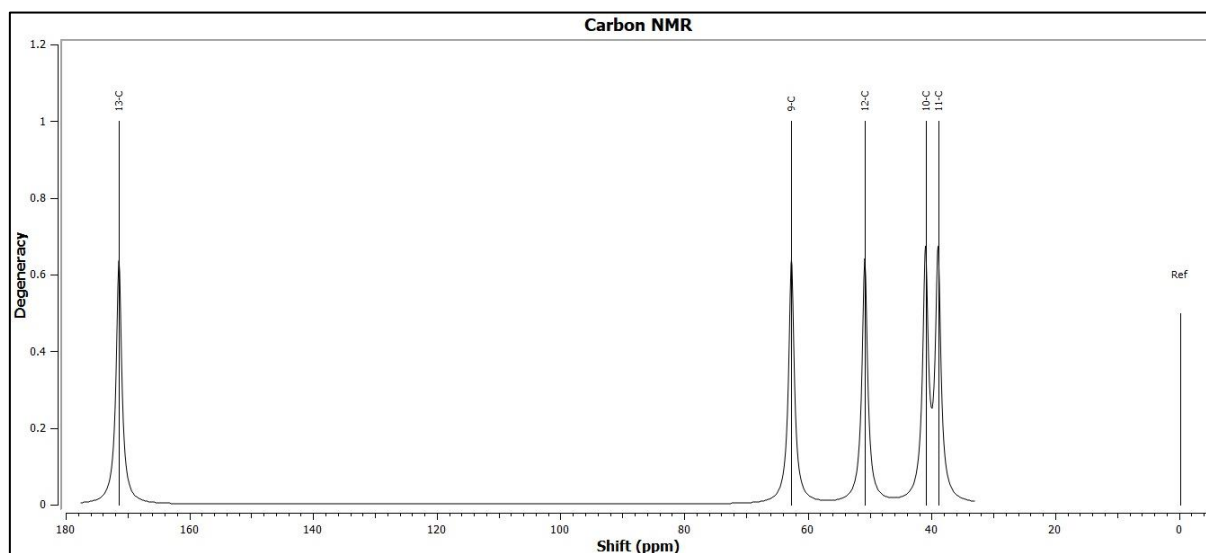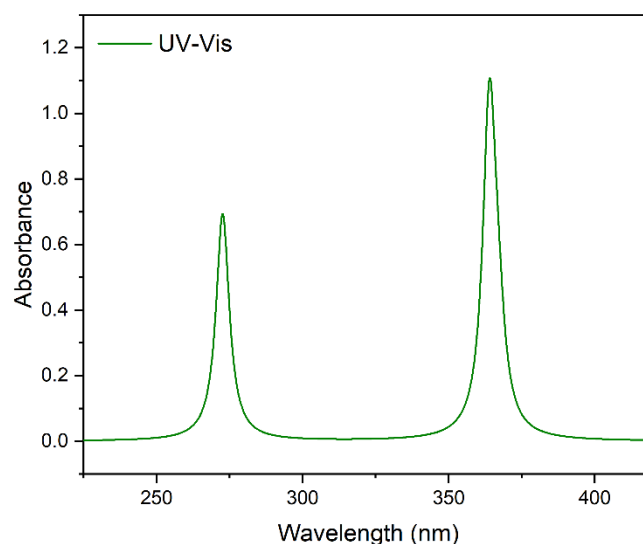**Figure 3 (a).** ^{1}H NMR spectrum of 1, 4-Dinitrosopiperazine-2-carboxylic acid

Figure 3 (b). 13C NMR spectrum of 1, 4-Dinitrosopiperazine-2-carboxylic acid

Table 3. Simulated chemical shift values (all values in ppm) of 1,4-Dinitrosopiperazine-2-carboxylic acid

Atoms	DFT	ChemDraw	Atoms	DFT	ChemDraw
H21	6.175	11.0	C13	171.400	174.7
H17	5.527	2.72	C9	62.748	71.7
H16	5.423	3.02	C12	50.900	53.1
H19	4.745	2.85	C10	41.096	53.6
H14	4.133	3.73	C11	39.059	50.8
H20	3.461	2.69	-	-	-
H15	2.884	2.77	-	-	-
H18	2.391	2.62	-	-	-

Figure 4. Electronic spectrum of 1,4-Dinitrosopiperazine-2-carboxylic acid

E HOMO = -7.0069 eV   E LUMO = - 2.0041 eV
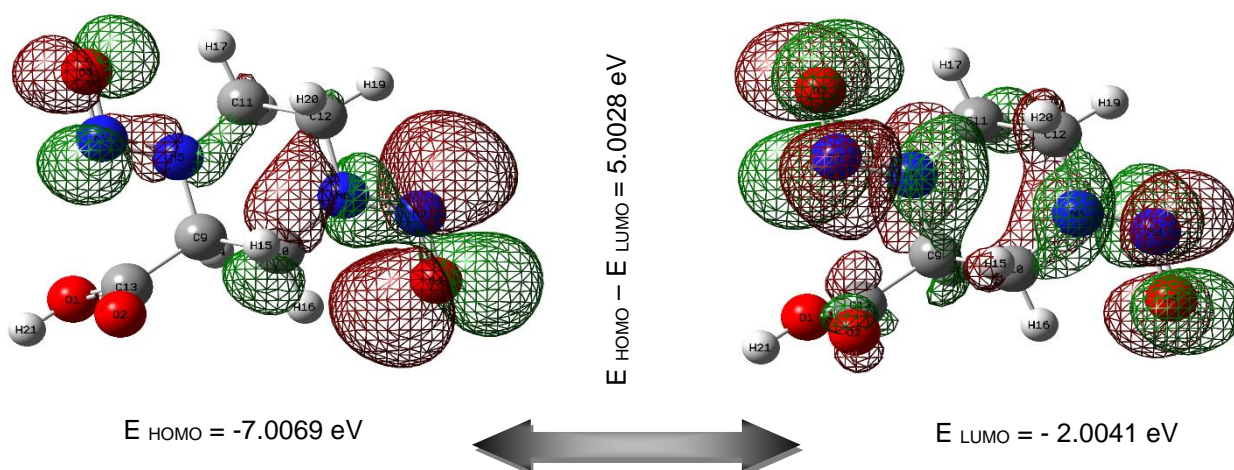
Figure 5. The HOMO-LUMO plots of 1,4-Dinitrosopiperazine-2-carboxylic acid

Table 4. Simulated wavelengths (λ), excitation energies (E), oscillator strengths (f), wavenumbers and major contributions of 1,4-Dinitrosopiperazine-2-carboxylic acid

λ (nm)	E (eV)	f	Wavenumber (cm^{-1})	Major contributions
367	3.3785	0.0003	27249.44	H-1→L+1 (15%), H→L (47%), H→L+1 (33%)
364	3.4063	0.0013	27474.03	H-1→L (66%), H-1→L+1 (10%), H→L+1 (23%)
273	4.5473	0.6923	36677.05	H→L (50%), H→L+1 (35%)

Table 5. The HOMO-LUMO energies and energy gap of 1,4-Dinitrosopiperazine-2-carboxylic acid

Parameters (eV)	TDDFT /B3LYP/ 6-311++G(d,p)
HOMO energy	- 7.0069
LUMO energy	- 2.0041
HOMO - LUMO energy gap	5.0028
HOMO-1 energy	- 7.1592
LUMO+1 energy	- 1.7760
(HOMO-1) - (LUMO+1) energy gap	5.3832
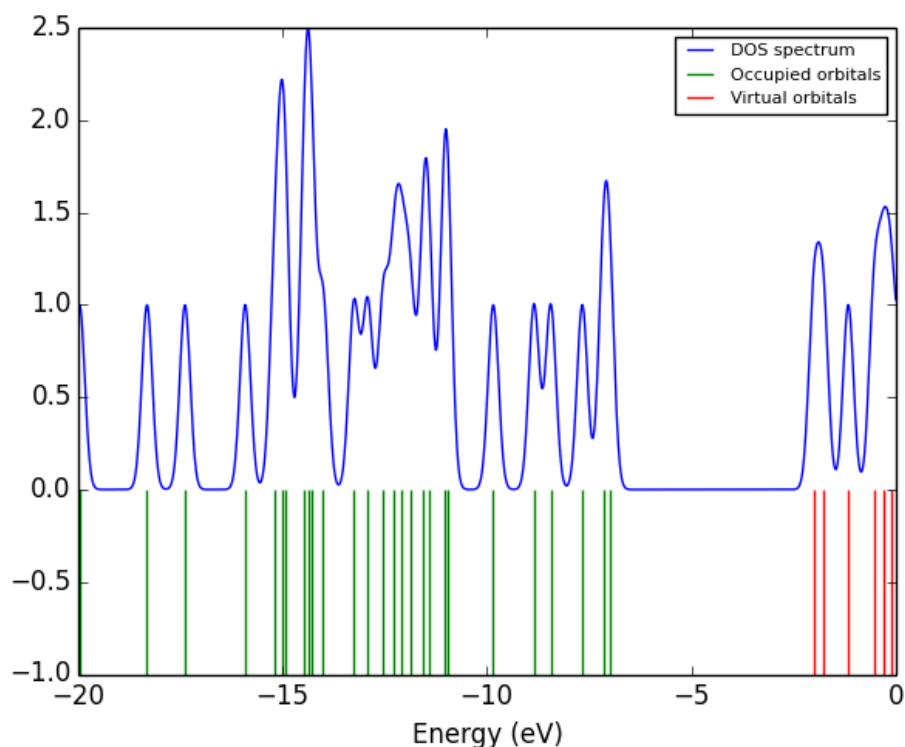
Figure 6. Density of states (DOS) spectrum of 1,4-Dinitrosopiperazine-2-carboxylic acid

The present investigation unveils the electronic properties of 1,4-Dinitrosopiperazine-2-carboxylic acid, focusing on absorption characteristics and energy gap. The first transition occurs at 367 nm with an excitation energy of 3.3785 eV and a moderate oscillator strength of 0.0003, suggesting a reasonably probable occurrence. The transition primarily involves electronic shifts from the highest occupied molecular orbital (H) to the lowest unoccupied molecular orbital (L), with contributions from adjacent orbitals. In the second transition at 364 nm with an excitation energy of 3.4063 eV, the oscillator strength notably increases to 0.0013, indicating a robust likelihood of occurrence. Here, electron movement from H-1 to L predominates, followed by contributions from other orbitals. The third transition at 273 nm with an excitation energy of 4.5473 eV displays an oscillator strength of 0.6923, indicating a relatively strong transition probability.

The primary electronic contributions involve electron shifts from H to L and H to L+1. Overall, these transitions signify the absorption of photons at specific energy levels, resulting in electron reorganization within the molecular orbitals. The electron-donating and accepting properties, as well as the optical characteristics, are markedly influenced by the HOMO-LUMO energy gap of 1,4-Dinitrosopiperazine-2-carboxylic acid. The HOMO-LUMO map employs red and green to delineate positive and negative regions within the molecule, respectively. The energy gap values in the gas phase are outlined in Table 5 and visually depicted in Figure 5. This gap is measured at 5.0028 eV and is graphically represented through density of states (DOS) spectrum in Figure 6. Within the DOS spectrum, occupied orbitals are highlighted in green, while unoccupied ones are depicted in red to enhance clarity and comprehension.

3.5. NBO Perspectives on Molecular Stabilization

NBO study presents the most precise representation of the "natural Lewis's structure" that is conceivable because all orbital features are quantitatively selected to incorporate the largest possible fraction of the electron density [44, 45]. With the help of DFT/B3LYP/6-311G++(d,p), the NBO properties of 1,4-Dinitrosopiperazine-2-carboxylic acid in the gas phase are simulated, and the values are presented in Table 6. From this table, the highest stabilization was found for the transition of LP (1) - σ* with the natural bonds of N6 → (O4-N8) with which the Electron Density is rising (ED = 0.006e) that affects the related bond N6 (ED = 1.599e) resulting in their stability as the energy of 76.50 kJ/mol. This signifies a significant electronic rearrangement in this interaction. The energy difference (0.21 a.u.) and polarized energy (0.114 a.u.) suggest a stable interaction. This high energy implies a potentially reactive site, where electron density is being redistributed. The next biggest interaction energy transitions were noted for LP (1) - σ* transition between the natural bonds of N5 and O3-N7 with an energy value

of 76.10 kJ/mol. Additionally, transitions with higher energy values, particularly those involving LP (2) - σ* interactions occurs between O3, O4 and N5-N7, N6-N8, contribute significantly to the stability of the molecule, with energy values of 22.23 and 22.10 kcal/mol respectively. Likewise, LP (1) - σ* interactions between nitrogen and carbon atoms (N7 – C11, N8 – C10) also make notable stability contributions, with energy values of 11.03 and 11.13 kcal/mol respectively. Moreover, this NBO study also assessed the quality of the natural Lewis structure for 1,4-Dinitrosopiperazine-2-carboxylic acid, relying on a total electron density ratio of 98.034%. This delineated the Lewis structure type at 98.034% and the non-Lewis structure type at 1.966%.

This comprehensive examination provides invaluable insights into the electronic structure and reactivity of 1,4-Dinitrosopiperazine-2-carboxylic acid, enhancing our understanding of its reactivity and behavior in chemical processes.

3.6. Mulliken Charge Distributions

In this study, a thorough simulation of the Mulliken charges for 1,4-Dinitrosopiperazine-2-carboxylic acid was conducted using the B3LYP/6-311++G(d,p) basis set, providing precise values detailed in Table 7. Additionally, these tabulated findings were supplemented with vivid graphical representations illustrating the electron population of individual atoms and the charge distribution across the molecule, as depicted in Figure 7. The Mulliken atomic charges for 1,4-Dinitrosopiperazine-2-carboxylic acid shed light on its electronic properties and reactivity. Oxygen atoms O1 (-0.723), O2 (-0.730), O3 (-0.662), and O4 (-0.641) exhibit negative charges, indicating their electron-donating potential. O1 and O2 demonstrate slightly higher electron density, potentially due to resonance effects or local environment factors. In contrast, carbon atoms C9 (0.244) to C13 (1.175) carry positive charges, signifying electron deficiency and a tendency to act as electron acceptors. Notably, C13 bears the highest positive charge, indicating pronounced electron deficiency.

Table 6. Second order perturbation theory of Fock matrix in selected NBO basis for 1,4-Dinitrosopiperazine-2-carboxylic acid

Donor (i)	Acceptor (j)	Type of Transition	Occupancy (ED/e)		Energy E$^{(2)}$ [a] kcal/mol	Energy difference E(j)-E(i) [b] a.u	Polarized energy F(i,j) [c] a.u
			Donor (i)	Acceptor (j)			
O1 – H21	C9 – C13	σ – σ*	1.985	0.073	3.86	1.09	0.059
C9 – C13	N5 – C11	σ – σ*	1.971	0.051	3.21	0.98	0.050
C9 – H14	O2 – C13	σ – σ*	1.965	0.022	3.04	1.14	0.053
C10 – H16	N5 – C9	σ – σ*	1.975	0.036	3.22	0.83	0.046
C10 – H16	N6 – C12	σ – σ*	1.975	0.027	4.37	0.85	0.054
C11 – H17	N5 – C9	σ – σ*	1.976	0.036	4.36	0.84	0.054
C12 – H19	N6 – C10	σ – σ*	1.977	0.049	4.48	0.85	0.055
O1	O2 – C13	LP (1) - σ*	1.975	0.207	7.61	1.25	0.087
O3	N5 – N7	LP (2) - σ*	1.897	0.085	22.23	0.66	0.108
O4	N6 – N8	LP (2) - σ*	1.900	0.084	22.10	0.66	0.108
N5	O3 – N7	LP (1) - σ*	1.603	0.006	76.10	0.21	0.114
N5	C9 – C10	LP (1) - σ*	1.603	0.026	4.60	0.62	0.053
N5	C9 – H14	LP (1) - σ*	1.603	0.024	4.90	0.66	0.056
N5	C11 – C12	LP (1) - σ*	1.603	0.021	4.17	0.63	0.051
N5	C11 – H18	LP (1) - σ*	1.603	0.017	4.75	0.66	0.056
N6	O4 – N8	LP (1) - σ*	1.599	0.006	76.50	0.21	0.114
N6	C9 – C10	LP (1) - σ*	1.599	0.026	4.32	0.61	0.051
N6	C10 – H15	LP (1) - σ*	1.599	0.017	5.01	0.67	0.057
N6	C11 – C12	LP (1) - σ*	1.599	0.021	4.27	0.62	0.051
N6	C12 – H20	LP (1) - σ*	1.599	0.021	5.15	0.65	0.058
N7	N5 – C11	LP (1) - σ*	1.946	0.051	11.03	0.78	0.083
N8	N6 – C10	LP (1) - σ*	1.954	0.049	11.13	0.79	0.084

[a] E(2) – Mean energy of hyper-conjugative interactions (stabilization energy).
[b] E(j)-E(i) – Energy difference between donor (i) and acceptor (j) natural bonding orbitals.
[c] F(i,j) – Fock matrix element between i and j natural bonding orbitals
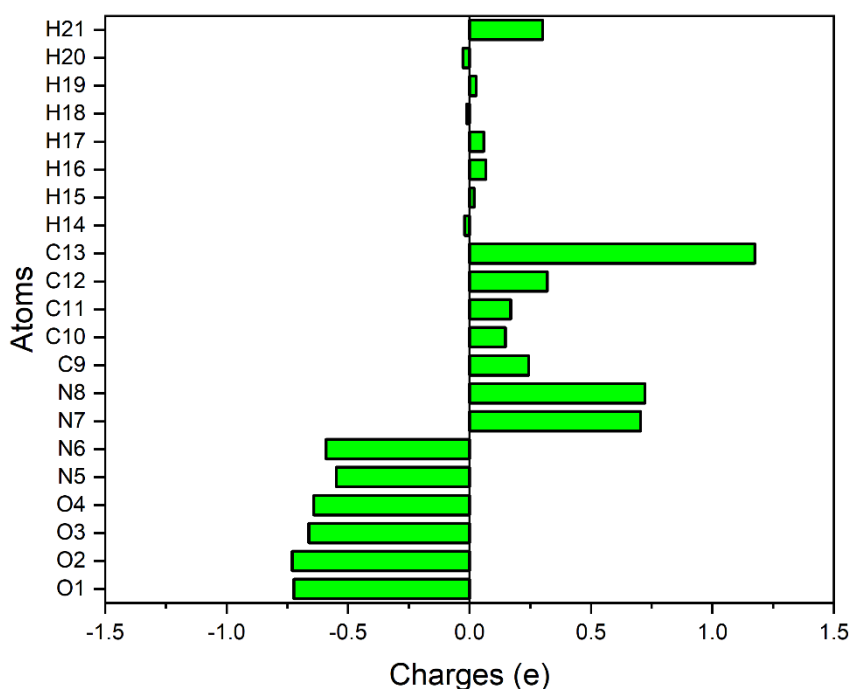
Figure 7. Mulliken charge distributions of 1,4-Dinitrosopiperazine-2-carboxylic acid

Table 7. Mulliken charge distributions of 1,4-Dinitrosopiperazine-2-carboxylic acid

Atom	Charges (e)	Atom	Charges (e)
O1	-0.723186	C12	0.320026
O2	-0.730485	C13	1.174963
O3	-0.661540	H14	-0.020638
O4	-0.641204	H15	0.019525
N5	-0.548973	H16	0.067149
N6	-0.591210	H17	0.059323
N7	0.704788	H18	-0.012124
N8	0.721849	H19	0.027415
C9	0.243540	H20	-0.027966
C10	0.148202	H21	0.300514
C11	0.170031	-	-

Nitrogen atoms N5 (-0.549) and N6 (-0.591) also show negative charges, highlighting their electron-donating nature. Nitrogen atoms N7 (0.705) and N8 (0.722) possess positive charges, suggesting their involvement in ionic interactions or significant roles in reactivity. Hydrogen atoms H14 (-0.021) to H21 (0.301) exhibit minimal charges, indicating a balanced electron distribution and a neutral role in electronic interactions. Furthermore, the comparison reveals that C9's positive charge is higher than that of N5 and N6, emphasizing its greater propensity to act as an electron acceptor

3.7. Molecular electrostatic potential surface

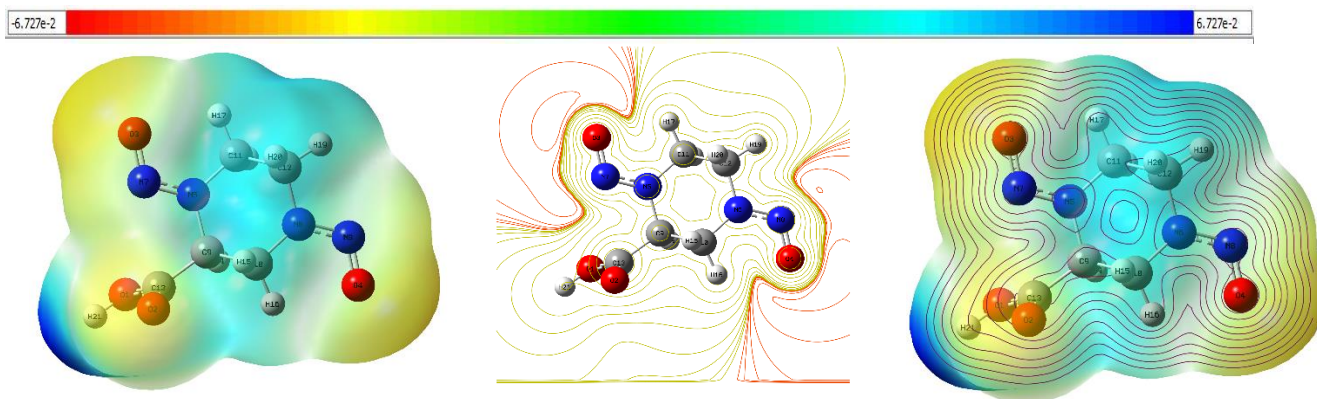The molecular electrostatic potential surface (MESP) is a valuable tool for evaluating electron density in a specific area around a molecule, providing valuable insights into potential nucleophilic and electrophilic reaction sites. The color-coded map offers a visual representation of the compound's characteristics, including its shape, chemical reactivity, size, charge density, and reactive regions [46, 47]. Colors like red, white, and blue on the map indicate electrophilic, neutral, and nucleophilic areas. In Figure 8, the electrostatic potential surface of 1,4-Dinitrosopiperazine-2-carboxylic acid is observed, with values ranging from -6.727×10^{-2} to 6.727×10^{-2} e.s.u. The surface visualization highlights areas with lower electron density, indicated by white regions surrounding the hydrogen atoms, which could potentially serve as binding sites for electrophilic reactive species. Conversely, areas rich in electrons, shown in red around the electronegative oxygen atom, may act as binding sites for nucleophilic reactive

species. These findings align closely with the results from the Mulliken population analysis.

3.8. Thermodynamic properties

The thermodynamic parameters for 1,4-Dinitrosopiperazine-2-carboxylic acid is presented in Table 8. The Self-Consistent Field (SCF) energy calculated as -715.318 *Hartree* signifies the electronic stability of 1,4-Dinitrosopiperazine-2-carboxylic acid in its ground state. The total thermal energy measured at 104.886 kcal mol^{-1} provides a comprehensive assessment of the overall energy content encompassing both electronic and thermal contributions. Vibrational energy at 103.109 kcal mol^{-1} characterizes the energy associated with molecular vibrational modes.

Figure 8. Total density and contour map with electrostatic potential surfaces of 1,4 Dinitrosopiperazine-2-carboxylic acid
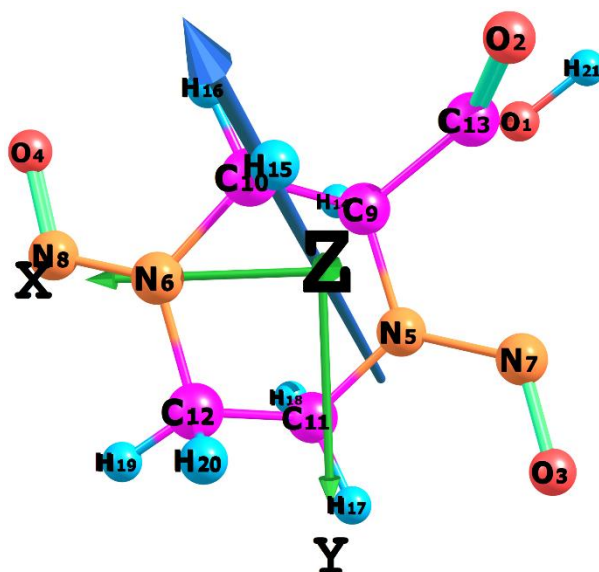
Figure 9. Direction of dipole moment vector of 1, 4-Dinitrosopiperazine-2-carboxylic acid

Table 8 . The calculated thermodynamical parameters of 1,4-Dinitrosopiperazine-2-carboxylic acid

Parameters	
SCF energy (Hartree)	-715.318
Total thermal energy (kcal mol^{-1})	104.886
Vibrational energy (kcal mol^{-1})	103.109
Zero-point vibrational energy (kcal mol^{-1})	97.431
Specific heat capacity, C_v (cal mol^{-1}K^{-1})	43.230
Entropy, S (cal mol^{-1} K^{-1})	111.199
Dipole Moment, μ (Debye)	
μ_x	-0.4037
μ_y	0.7423

μ_z	-1.3524
μ_{total}	1.5947
Rotational Constants (GHz)	
X	1.12531
Y	0.63765
Z	0.45178

The zero-point vibrational energy calculated at 97.431 kcal mol^{-1} represents the theoretical lower limit of vibrational motion at absolute zero temperature. The specific heat capacity (C_V) evaluated at 43.230 cal mol^{-1} K^{-1} sheds light on the molecule's ability to absorb thermal energy. Entropy (S) measuring molecular disorder is computed at 111.199 cal mol^{-1} K^{-1} emphasizing the molecule's notable degree of flexibility and motion. The dipole moment (μ) exhibits a notable degree of asymmetry in its charge distribution. This is evident from the individual components of the dipole moment along the x, y, and z axes. These values indicate that the dipole moment does not align with any specific Cartesian axis, suggesting a complex three-dimensional charge distribution within the molecule, which is illustrated in Figure 9. The total dipole moment (μ_{total}) of 1.5947 Debye signifies significant polarity, influencing the molecule's chemical behavior in diverse contexts due to its extensive charge separation. Finally, the rotational constants (X, Y, and Z) of 1.12531, 0.63765, and 0.45178 *GHz*, respectively, furnish crucial insights into the molecule's rotational characteristics. Together, these parameters offer a foundational understanding of the energetic profile and dynamic behavior of 1,4-Dinitrosopiperazine-2-carboxylic acid providing a basis for further computational investigations in theoretical chemistry.

4. Conclusion

This comprehensive computational study yields several prominent findings regarding 1,4-Dinitrosopiperazine-2-carboxylic acid. The optimized geometry reveals intriguing bond lengths and angles, with distinctive values such as the C-O-H angle at 107.85º and the O-C bond lengths ranging from 1.201 to 1.345 Å. These values underscore the molecule's unique structural intricacies. Vibrational analysis uncovers dynamic interactions, with notable peaks such as the strong stretching vibration of the hydroxyl group at 3753 cm^{-1}, indicating its significant role in intermolecular interactions. The simulated chemical shifts provide crucial insights, particularly the hydroxyl proton at 6.175 ppm, indicative of a distinctive electronic environment. Electronic property analysis reveals key transitions, with the first transition at 367 nm and excitation energy of 3.3785 eV, signifying an energetically probable occurrence. The NBO study highlights crucial stabilizing interactions, particularly the LP (1) - σ* transition with an energy of 76.50 kJ/mol, indicating a site of potential reactivity. Mulliken charges reveal electron-donating and accepting nature of specific atoms, influencing reactivity, exemplified by the positive charges on carbon atoms C9 to C13. The MESP and its color-coded map offer essential insights into electron density and reactive sites, which aligns with Mulliken population analysis results. Finally, thermodynamic properties provide a comprehensive energy profile, including a total thermal energy of 104.886 kcal mol^{-1} and a dipole moment of 1.5947 Debye, signifying significant polarity. These findings not only deepen our understanding of 1,4-Dinitrosopiperazine-2-carboxylic acid but also pave the way for further computational investigations with potential applications in materials science and pharmaceuticals. This study stands as a crucial contribution to the field, filling a critical gap in existing literature and providing essential knowledge for harnessing the compound's full potential.

References

[1]   C.L. Allen, A.R. Chhatwal, J.M. Williams, Direct amide formation from unactivated carboxylic acids and amines. Chemical Communications, 48(5), (2012) 666-668. https://doi.org/10.1039/C1CC15210F

[2]   A.S. Kalgutkar, J.S. Daniels, Carboxylic acids and their bioisosteres. Metabolism, Pharmacokinetics and Toxicity of Functional Groups: Impact of Chemical Building Blocks on ADMET. Royal Society of Chemistry, 9, (2010) 99-167.

[3]   C. Florindo, F.S. Oliveira, L.P. Rebelo, Fernandes, A.M, Marrucho, I.M. Insights into the synthesis and properties of deep eutectic solvents based on cholinium chloride and carboxylic acids. ACS Sustainable Chemistry & Engineering, 2(10) (2014) 2416-25. https://doi.org/10.1021/sc500439w

[4]   M.K. Akhtar, N.J. Turner, P.R. Jones, Carboxylic acid reductase is a versatile enzyme for the conversion of fatty acids into fuels and chemical commodities. Proceedings of the National Academy of Sciences, 110(1) (2013) 87-92. https://doi.org/10.1073/pnas.1216516110

[5]   Y. Huang, T. Ma, Q. Wang, C. Guo, Synthesis of biobased flame-retardant carboxylic acid curing agent and application in wood surface coating. ACS Sustainable Chemistry & Engineering, 7(17), (2019) 14727-14738.

https://doi.org/10.1021/acssuschemeng.9b02645

[6] C. Ballatore, D.M. Huryn, A.B. Smith, 3rd. Carboxylic acid (bio)isosteres in drug design. ChemMedChem. 8(3), (2013) 385-395. https://doi.org/10.1002/cmdc.201200585

[7] N.A. Fine, M.J. Goldman, P.T. Nielse, G.T. Rochelle, Managing n-nitrosopiperazine and dinitrosopiperazine. Energy procedia, 37 (2013) 273-284. https://doi.org/10.1016/j.egypro.2013.05.112

[8] A.K. Rathi, R. Syed, H.S. Shin, R.V. Patel, Piperazine derivatives for therapeutic use: a patent review (2010-present). Expert opinion on therapeutic patents, 26(7), (2016) 777-797. https://doi.org/10.1080/13543776.2016.1189902

[9] F. Tang, F. Zou, Z. Peng, D. Huang, Y. Wu, Y. Chen, C. Duan, Y. Cao, W. Mei, X. Tang, Z. Dong, N,N´-Dinitrosopiperazine-mediated Ezrin Protein Phosphorylation via Activation of Rho Kinase and Protein Kinase C Is Involved in Metastasis of Nasopharyngeal Carcinoma 6-10B Cells. Journal of Biological Chemistry, 286(42), (2011) 36956-36967. https://doi.org/10.1074/jbc.M111.259234

[10] Y. Li, J. Lu, S. Zhou, W. Wang, G. Tan, Z. Zhang, Z. Dong, T. Kang, F. Tang, Clusterin induced by N, N´-Dinitrosopiperazine is involved in nasopharyngeal carcinoma metastasis. Oncotarget, 7(5), (2016) 5548-5563. https://doi.org/10.18632/oncotarget.6750

[11] Y. Li, K. Ju, W. Wang, Z. Liu, H. Xie, Y. Jiang, G. Jiang, J. Lu, Z. Dong, F. Tang, Dinitrosopiperazine-decreased PKP3 through upregulating miR-149 participates in nasopharyngeal carcinoma metastasis. Molecular carcinogenesis, 57(12), (2018) 1763-1779. https://doi.org/10.1002/mc.22895

[12] Z. Peng. N. Liu, D. Huang, C. Duan, Y. Li, X. Tang, W. Mei, F. Zhu, F. Tang, N, N'-dinitrosopiperazine–mediated heat-shock protein 70-2 expression is involved in metastasis of nasopharyngeal carcinoma. PLoS one, 8(5) (2013) e62908. https://doi.org/10.1371/journal.pone.0062908

[13] D. Huang, Y. Li, N. Liu, Z. Zhang, Z. Peng, C. Duan, X. Tang, G. Tan, G. Yan, F. Tang, Identification of novel signaling components in N, N'-Dinitrosopiperazine-mediated metastasis of nasopharyngeal Carcinoma by quantitative phosphoproteomics. Bmc Cancer, 14, (2014) 1-15. https://doi.org/10.1186/1471-2407-14-243

[14] G. Tan, X. Tang, D. Huang, Y. Li, N. Liu, Z. Peng, Z. Zhang, C. Duan, J. Lu, G. Yan, F. Tang,

Dinitrosopiperazine-mediated phosphorylated-proteins are involved in nasopharyngeal carcinoma metastasis. International Journal of Molecular Sciences, 15(11), (2014) 20054-20071. https://doi.org/10.3390/ijms151120054

[15] N. Yaghmaeiyan, A. Bamoniri, M. Mirzaei, (2022). The stereochemistry study of N, N-dinitrosopiperazine using 1H NMR technique. Preprint https://doi.org/10.21203/rs.3.rs-2071349/v1

[16] M.J. Frisch, *et al.,* (2009). GAUSSIAN09. Gaussian Inc., Wallingford, CT, USA.

[17] W. Kohn, L.J. Sham, Self-consistent equations including exchange and correlation effects, Physical Review, 140(4A), (1965) A1133-A1138. https://doi.org/10.1103/PhysRev.140.A1133

[18] A.D. Becke, Density functional thermo chemistry – III: The role of exact exchange. The Journal of Chemical Physics, 98 (1993) 5648-5652. https://doi.org/10.1063/1.464913

[19] C. Lee, W. Yang, R.G. Parr, Development of the Colle-Salvetti correlation-energy formula into a functional of the electron density. Physical Review B, 37 (1988) 785-789. https://doi.org/10.1103/PhysRevB.37.785

[20] W.J. Hehre, R. Ditchfield, J.A. Pople, Self-Consistent Molecular Orbital Meth- ods. XII. Further Extensions of Gaussian—Type Basis Sets for Use in Molecular Orbital Studies of Organic Molecules. The Journal of Chemical Physics, 56(5), (1972) 2257–2261. https://doi.org/10.1063/1.1677527

[21] J.R. Cheeseman, G.W. Trucks, T.A. Keith, & M.J. Frisch, A comparison of models for calculating nuclear magnetic resonance shielding tensors. The Journal of Chemical Physics, 104 (1996) 5497–5509. https://doi.org/10.1063/1.471789

[22] M. Petersilka, U.J. Gossman, E.K.U. Gross, Excitation energies from timed-ependent density-functional theory. Physical Review Letters, 76 (1966) 1212-1215. https://doi.org/10.1103/PhysRevLett.76.1212

[23] E. Runge, E.K.U. Gross, Density functional theory for time-dependent systems. Physical Review Letters, 52 (1984) 997. https://doi.org/10.1103/PhysRevLett.52.997

[24] G.A. Zhurko, D.A. Zhurko, Chemcraft Program Version 1.6 (Build 315), (2009).

[25] N.B. Arslan, N. Özdemir, O. Dayan, N. Dege, M. Koparır, P. Koparır, H. Muğlu, Direct and solvent-assisted thione–thiol tautomerism in 5-(thiophen-2-yl)-1, 3, 4-oxadiazole-2 (3H)-thione: Experimental and molecular modeling study.

Chemical Physics, 439, (2014) 1-11. https://doi.org/10.1016/j.chemphys.2014.05.006

[26] M. Shkir, Investigation on the key features of L-Histidinium 2-nitrobenzoate (LH2NB) for optoelectronic applications: a comparative study. Journal of King Saud University-Science, 29 (1), (2017) 70-83. https://doi.org/10.1016/j.jksus.2016.03.002

[27] S. Omar, S. Mohd, M. Ajmal Khan, Z. Ahmad, S. AlFaify, A comprehensive study on molecular geometry, optical, HOMO-LUMO, and nonlinear properties of 1, 3-diphenyl-2-propen-1-ones chalcone and its derivatives for optoelectronic applications: a computational approach. Optik, 204 (2020) 164172. https://doi.org/10.1016/j.ijleo.2020.164172

[28] S.D. Kanmazalp, M. Macit, N. Dege, Hirshfeld surface, crystal structure and spectroscopic characterization of (E)-4-(diethylamino)-2-((4-phenoxyphenylimino) methyl) phenol with DFT studies. Journal of Molecular Structure, 1179, (2019) 181-191. https://doi.org/10.1016/j.molstruc.2018.11.001

[29] B. Himmi, S.A. Brandán, Y. Sert, A.A. Kawther, N. Dege, E.B. Cinar, A.E. Louzi, K. Bougrin, K. Karrouchi, A quinoline-benzotriazole derivative: Synthesis, crystal structure and characterization by using spectroscopic, DFT and molecular docking methods. Results in Chemistry, 5 (2023) 100916. https://doi.org/10.1016/j.rechem.2023.100916

[30] F. El Kalai, E.B. Çınar, Y. Sert, M. Alhaji Isa, C.H. Lai, F. Buba, N. Benchat, K. Karrouchi, Synthesis, crystal structure, DFT, Hirshfeld surface analysis, energy framework, docking and molecular dynamic simulations of (E)-4-(4-methylbenzyl)-6-styrylpyridazin-3 (2H)-one as anticancer agent. Journal of Biomolecular Structure and Dynamics, (2023). 1-20. https://doi.org/10.1080/07391102.2022.2164796

[31] S. Selvaraj, In Silico Studies on the Molecular Geometry, FMO, Mulliken Charges, MESP, ADME and Molecular Docking Prediction of Pyrogallol Carboxaldehydes as Potential Anti-tumour Agents. Physical Chemistry Research, 12(2), (2024) 305-320. https://doi.org/10.22036/PCR.2023.402835.2359

[32] M. Arıcı, O.Z. Yeşilel, E. Acar, N. Dege, Synthesis, characterization and properties of nicotinamide and isonicotinamide complexes with diverse dicarboxylic acids, Polyhedron, 127, (2017) 293-301. https://doi.org/10.1016/j.poly.2017.02.013

[33] S. Kansız, N. Dege, Synthesis, crystallographic structure, DFT calculations and Hirshfeld surface analysis of a fumarate bridged Co (II) coordination polymer. Journal of Molecular Structure, 1173 (2018) 42-51. https://doi.org/10.1016/j.molstruc.2018.06.071

[34] K. Guna, P. Sakthivel, I. Ragavan, A. Arunkumar, P.M. Anbarasan, M. Shkir, An experimental and computational analysis on 2, 6-diamine-7H-purine ligand with spectroscopic, AIM, NLO and biological activity. Optics & Laser Technology, 168 (2024) 109872. https://doi.org/10.1016/j.optlastec.2023.109872

[35] P. Rajkumar, S. Selvaraj, R. Suganya, M. Kesavan, G. Serdaroğlu, S. Gunasekaran, S. Kumaresan, Experimental and theoretical investigations on electronic structure of 5-(hydroxymethyl)-2-furaldehyde: An antisickling agent identified from terminalia bellirica. Chemical Data Collections, 29, (2020) 100498. https://doi.org/10.1016/j.cdc.2020.100498

[36] Y. Ait Elmachkouri, Y. Sert, E. Irrou, E. H. Anouar, H. Ouachtak, J.T. Mague, N.K. Sebbar. M.L. Taha, Synthesis, X-Ray Diffraction, Spectroscopic Characterization, Hirshfeld Surface Analysis, Molecular Docking Studies, and DFT Calculation of New Pyrazolone Derivatives. Polycyclic Aromatic Compounds, (2023) 1-22. https://doi.org/10.1080/10406638.2023.2219804

[37] G. Serdaroglu, Experimental and theoretical spectroscopic studies of the electronic structure of 2-ethyl-2-phenylmalonamide. Physical Chemistry Research, 10(3), (2022) 333-344.

[38] D. Kattan, M.A. Palafox, S.K. Rathor, V.K. Rastogi, A DFT analysis of the molecular structure, vibrational spectra and other molecular properties of 5-nitrouracil and comparison with uracil. Journal of Molecular Structure, 1106, (2016) 300-315. https://doi.org/10.1016/j.molstruc.2015.10.096

[39] M.A. Palafox, D. Bhat, Y. Goyal, S. Ahmad, I.H. Joe, V.K. Rastogi, FT-IR and FT-Raman spectra, MEP and HOMO–LUMO of 2, 5-dichlorobenzonitrile: DFT study. Spectrochimica Acta Part A: Molecular and Biomolecular Spectroscopy, 136, (2015) 464-472. https://doi.org/10.1016/j.saa.2014.09.058

[40] K. Subashini, S. Periandy, Spectroscopic (FT-IR, FT-Raman, UV, NMR, NLO) investigation, molecular docking and molecular simulation dynamics on 1-Methyl-3-Phenylpiperazine. Journal of Molecular Structure, 1143 (2017) 328-343. https://doi.org/10.1016/j.molstruc.2017.04.016

[41] E. Jaziri, H. Louis, C. Gharbi, F. Lefebvre, W. Kaminsky, E.C. Agwamba, T.C. Egemonye, T.O.

Unimuke, O.J. Ikenyirimba, G.E. Mathias, C.B. Nasr, L. Khedhiri, Investigation of crystal structures, spectral (FT-IR and NMR) analysis, DFT, and molecular docking studies of novel piperazine derivatives as antineurotic drugs. Journal of Molecular Structure, 1278 (2023) 134937.
https://doi.org/10.1016/j.molstruc.2023.134937

[42] S. Selvaraj, A.R. Kumar, T. Ahilan, M. Kesavan, S. Gunasekaran, S. Kumaresan, Multi spectroscopic and computational investigations on the electronic structure of oxyclozanide. Journal of the Indian Chemical Society, 99(10), (2022) 100676.
https://doi.org/10.1016/j.jics.2022.100676

[43] N.E. Safronov, I.P. Kostova, M.A. Palafox, N.P. Belskaya, Combined NMR Spectroscopy and Quantum-Chemical Calculations in Fluorescent 1, 2, 3-Triazole-4-carboxylic Acids Fine Structures Analysis. International Journal of Molecular Sciences, 24(10), (2023) 8947.
https://doi.org/10.3390/ijms24108947

[44] N. Uludag, G. Serdaroğlu, P. Sugumar, P. Rajkumar, N. Colak, E. Ercag, Synthesis of thiophene derivatives: Substituent effect, antioxidant activity, cyclic voltammetry, molecular docking, DFT, and TD-DFT calculations. Journal of Molecular Structure, 1257, (2022)132607.
https://doi.org/10.1016/j.molstruc.2022.132607

[45] S. Sundari, A. Muthuraja, S. Chandra, P. Rajkumar, Spectroscopic analysis (FT-IR/FT-Raman), electronic (UV–visible), NMR and docking on 4-methoxyphenylboronic acid (4MPBA) by DFT calculation. Molecular Crystals and Liquid Crystals, 755(1), (2023) 23-40.
https://doi.org/10.1080/15421406.2022.2100965

[46] A.R. Kumar, S. Selvaraj, P. Anthoniammal, R.J. Ramalingam, R. Balu, P. Jayaprakash, G.P.S. Mol, Comparison of spectroscopic, structural, and molecular docking studies of 5-nitro-2-fluoroaniline and 2-nitro-5-fluoroaniline: An attempt on fluoroaniline isomers. Journal of Fluorine Chemistry, 270, (2023) 110167.
https://doi.org/10.1016/j.jfluchem.2023.110167

[47] A. Asha, P. Jayaprakash, S. Selvaraj, D.P. Matharasi, P. Rajkumar, Growth, spectral and quantum chemical investigations on N-butyl-4-nitroaniline single crystal for nonlinear optical and optoelectronic device applications. Journal of Materials Science: Materials in Electronics, 34(10), (2023) 895.
https://doi.org/10.1007/s10854-023-10292-2

Competing Interests

The author declares that there are no conflicts of interest regarding the publication of this manuscript.

Data Availability

Data will be provided upon request.

Has this article screened for similarity?

Yes